Supplemental Materials

Molecular Biology of the Cell

Julius et al.

SUPPLEMENTAL MATERIAL

SUPPLEMENTAL RESULTS

CEN Duplication in Budding Yeast Treated with HU

In budding yeast, mutations that disrupt K-MT attachment or the *CEN* linkages between sister Ks lead to aberrant spindle structure and defective extension, revealing the importance of amphitelicK attachmentsin spindle organization andlength regulation(Goh and Kilmartin, 1993; Goshima *et al.*, 1999; Jones *et al.*, 1999; Skibbens *et al.*, 1999; Severin *et al.*, 2001; Bachant *et al.*, 2002; Gardner *et al.*, 2005; Bouck and Bloom, 2007; Romao *et al.*, 2008; Warsi *et al.*, 2008; Yeh *et al.*, 2008; Stephens *et al.*, 2011, 2013; Nannas *et al.*, 2014; Lawrimore *et al.*, 2016). K function is similarly important in preventing aberrant spindle extension in HU arrested cells(Bachant *et al.*, 2005; Ma *et al.*, 2007; Liu *et al.*, 2008), raising the questionof to what extentamphitelicK attachments are able to form in early S phase. While this is an important issue with respect to spindle structure during early S phase, the inability to directly visualize yeast K-MT attachments makesit adifficult one to address experimentally. In metaphase spindles, C-loop formation-which can be readily visualized as paired foci of *CEN* chromatin(Goshima and Yanagida, 2000; He *et al.*, 2000; Tanaka *et al.*, 2000)-provides a convenient readout foramphitelicK attachment. Such paired foci are not typically observed in HU treated cells, potentially providing support for the idea that amphitelic K attachments cannot occur in early S phase(Krishnan *et al.*, 2004; Liu *et al.*, 2008). This interpretation is problematic, however, in that the specialized cohesive properties of the C-loop may have not yet formedduring the early period of HU treatment, with duplicated *CEN*S more likely tobe linked through DNA topology-for example in the context of a catenated replication bubble.

A different approach is to therefore to examine the extent and kinetics of *CEN* duplication in HU, providing insight intothe capacity for amphitelicK attachments. Here too there are open questions. On the one hand, since all 16 *CEN*s are flanked by efficient *ORI*s that are among the first to fire in S phase(Raghuraman *et al.*, 2001; Yabuki *et al.*, 2002; Feng *et al.*, 2006; Crabbé *et al.*, 2010), it seems

probable that forks would be able to traverse *CEN*s prior to nucleotide depletion. On the other, at least two reports have suggested that the number of *CEN*s that are replicated during the first two hours of HU treatment-the period during which the spindle assembles-is likely to be small(Feng *et al.*, 2009; Poli *et al.*, 2012). Analyses of replication tracks in HU treated yeast have shown that most forks advance 2000-6000 bp before dNTPs become limiting(Poli *et al.*, 2012), although a number of forks can advance up to 17kbp(Lopes *et al.*, 2001). In comparison, the distances separating all 16 *CEN*s from their respective 32 flanking *ORI*s ranges between 187-22,887 bp (average, 10,652 bp) for the replication profiles reported here (Supplemental Figure4B, Supplemental Tables 1 and 2), and between 422-110,382 bp (average, 20,031 bp) for the data published by Yabuki*et al.*, 2002 (Supplemental Table 4). In general, these considerations suggest the duplication of many *CEN*s is likely to be probabilistic during the initial S phase delay imposed by HU, and the actual number of *CEN*s duplicated per cell at a given time will therefore vary throughout the population. Given these considerations, we decided to undertake a statistical analysis ofthe probability and kinetics of *CEN* duplication in HU.

Assumptions and modeling

We used two sources of data for our calculations: the S/G_1 ssDNA ratios for *Δdbf4/pDBF4*cells generated in this report and the quantitative hybridization dataset described for HU treated WT cells by Yabuki*et al*., 2002. For our data, we wished to compare the probability of *CEN* duplication in *Δdbf4/pDBF4*cells treated with HU to *Δdbf4/pdbf4-zn*cells, where utilization of *CEN*-proximal *ORI*s is strongly reduced. An additional consideration was that the requirement for Pds1 to restrain spindle extension in HU has been reported to become operative between 180-240 min of HU treatment(Clarke *et al.*, 2001). As discussed in this report (Discussion and Supplemental Figure 9) we were interested in the possibility that a distinct S phase mode of spindle organization in HU transitions into a canonical metaphase spindle where structural stability/length regulation becomes reliant on the Pds1 block to

cohesin proteolysis. If there is such a transition, the kinetics of *CEN* duplication during an extended HU treatment is of interest. We therefore modeled the kinetics of *CEN* duplication over a 60-300 min simulated HU treatment. 300 min was chosen as an end point because at this time WT cells treated with 200 mM HU have largely circumvented the HU block as evaluated by FACs and will soon proceed into anaphase (data not shown). The dataset from Yabuki et al., 2002 was included because an advantage of this study is that hybridization values are directly proportional to DNA synthesis.

Our approach was based on treating ssDNA replication profiles as probability distributions for bi-directional fork movement away from an *ORI*. Replication forks appear to advance at a slow but constant rate following nucleotide depletion in HU(Poli *et al.*, 2012), and weassumed this rate could be used to extrapolate fork distributions forward in time. An additional assumption was that relative differences in replication profile amplitude reflect differences in *ORI* utilization in the particular S phase captured by the experiment. Finally, since budding yeast *CEN*s are only ~150 bp in length, we considered it reasonable to approximate them as completely replicated or un-replicated points. Given these assumptions, the main task became to use the data in the replication profiles to derive p(*CEN*)t, the probability of a *CEN* being duplicated by a fork from any of a set of proximal *ORI*s at time (t) following G_1 release into 200 mM HU. The p(*CEN*)t values for all 16 chromosomes were then combined to derive two informative statistics. The first was p(at least N)t, the fraction of the cell population containing at least N duplicated *CEN*s at time (t). Determining p(at least N)t involved computing the individual probabilities of all 65,535 combinations of 16 *CEN*s taken N at a time, with N ranging from 1 to 16. The probability of each combination was then subtracted from 1. The product of all members of this complementary set is the probability that none of the duplication combinations will have occurred at time (t), which we denote as p(none of *C*(16,N)t). The probability of at least one combination occurring is then:

1. p(at least N)t = 1 - [p(none of *C*(16,N)t)]

The second statistic was p(N)t, the fraction of the cell population containing N duplicated *CEN*s. p(N)t was solved according to equation 2.

2. p(N)t = p[at least N]t–p[at least (N +1)]t, with p(at least 0)=1 and p(at least 17)=0.

ssDNA dataset calculations

In WT cells, ssDNA associated with HU exposure is restricted to a short (~300 bp) region immediately adjacent to replication forks(Lopes *et al.*, 2001). In ssDNA replication profiles, this signal typically manifests itself as a split peak with maximal amplitudes +/- 3000 bp from *ORI* centers and a range of +/- 17,000 bp along the chromosome axis (Figure 6A, Supplemental Figures 2 and 3). These distances are in good agreement with the average and maximal extent of fork advance in HU as determined by 2D gel and combing analyses(Lopes *et al.*, 2001; Poli *et al.*, 2012). To derive p(*CEN*)t values, we first generated a composite profile of the 16 *ORI*s closest to each *CEN*from the *Δdbf4/pDBF4*dataset (Figure 7A). Using this composite, the cumulative area associated with 1000 bp intervals at progressively closer distances to the *ORI* center was quantified and expressed as a fraction of the total area encompassed by leftward or rightward forks. Integrating the profiles in this fashion yielded probability curves for fork advance in either direction, reaching an internally normalized value of 1 at the *ORI* center (Supplemental Figure 5A). 5^{th} order polynomial equations were fitted to the probability curves.

In HU treated cells, nucleotide exhaustion occurs by 30 min, after which forks advance at a reduced but constant rate (80 bp/min) for several hours(Poli *et al.*, 2012). By applying this constant rate, we projected the polynomial curve fit for the *Δdbf4/pDBF4*replication compositein both directions from the *ORI* center, starting at the 60 min sampling time out to the desired 300 min end point of the

simulation (Supplemental Figure 5A). Notably, this treatment considers continued DNA synthesis in HU as solely due to advance of existing forks at a constant rate. Based on current information, by 60 min unchecked *ORI*s are expected to have fired according to their intrinsic efficiencies, while firing of additional *ORI*s will be blocked through activation of Rad53(Santocanale and Diffley, 1998; Feng *et al.*, 2006; Crabbé *et al.*, 2010; Poli *et al.*, 2012). However, with extended time in HU, nucleotide pool expansion should eventually allow forks to return to a more normal rate of synthesis, and the pace of the temporal program of *ORI* firing will begin to increase. Thus, our approach may progressively under-represent *CEN* duplication at the simulation continues.

p(*CEN*)t values were calculated in three steps. A first step was to identify all possible *ORI*s that, based on the maximal extent of fork advance in our projections, could conceivably contribute to *CEN* duplication during the 300 min simulation, leading us to select a total of 45 *ORI*s +/- 35,000 bp on either side of all 16 *CEN*s. Using the polynomial equations and the relevant *CEN*-*ORI* distances, the probability of a fork from each of the proximal *ORI*s traversing a *CEN* could be determined over the 60-300 min time frame. The second step was to assign relative values for *ORI* utilization for each of the 45 ORIs, ranging from 0 to 1. As *CEN* duplication in our model was influenced by how *ORI* utilization values were specified, the outcome of several approaches will be described. In all cases, the probability of fork traversal was multiplied by the *ORI* utilization value to yield the probability of the *CEN* actually being duplicated by a fork emanating from this *ORI*, denoted as p(dup)t. In a third and final step, each p(*CEN*)t value was calculated as the probability of a *CEN* being duplicated by any of the selected proximal *ORI*s on that chromosome. To do this, it was assumed that the slow rate of fork progression in HU allows the firing of the 45 *ORI*s to be treated as independent events. In this case, the product of all [1 – p(dup)t] values for any set of p(dup)t is the probability that none of the forks under consideration will have traversed the *CEN* at (t). Subtracting this value from 1 yields p(*CEN*)t, the probability that at least one of the forks will traverse the *CEN*. The 16 p(*CEN*)t values for 15-30 min treatment intervals were then

combined according to equations 1 and 2 to yield p(at least N)t and p(N)t statistics over the simulated 60-300 min period (Figure 7B, Supplemental Figure 5B and Supplemental Table 5).

ORIutilization values based on normalization to maximum non-outlier area. In this simulation, relative values for *ORI* utilization were assigned by normalizing the areas under ssDNA *ORI*peaks (*ORI*AUCs) for all 177*ORI*s that fire in the *Δdbf4/pDBF4*data set to the largest *ORI*AUC that was not a statistical outlier (Q3 + 1.5*IQR). Outlier *ORI*s with relative utilization values > 1.0, including *CEN*-flanking ARS606 and ARS1309, were set to 1. This normalization procedure yielded an average utilization score of 0.48 for the 45 *ORI*s that were included in the simulation, which is consistent with other estimates for average *ORI* efficiency(Friedman *et al.*, 1997; Yamashita *et al.*, 1997; Luo *et al.*, 2010). To obtain *ORI* utilization values for *Δdbf4/pdbf4-zn*, we first divided *Δdbf4/pdbf4-znORI*AUCs for the 45 *ORI*s by the corresponding *Δdbf4/pDBF4ORI*AUC as described in Figure 6B and Supplemental Figure 4A. These ratios were then multiplied by the relative *ORI* utilization values in *Δdbf4/pDBF4*cells, reducing the average *ORI* utilization to 0.18 for the *Δdbf4/pdbf4-zn*mutant. Supplemental Tables1 and 2 list the identity, *CEN-ORI* distance, *Δdbf4/pdbf4-znORI*AUC ratios (Supplemental Table 2) and relative utilization values (RelE) for all 32 *CEN* flanking *ORI*s that were determined using this approach, as well as the p(*CEN*)t values that were obtained. Figure 7Bdisplays the minimum number of duplicated *CEN*s expected to occur in≥ 98% of *Δdbf4/pDBF4*and *Δdbf4/pdbf4-zn*cells over 60-300 min [p(at least N)t values]. p(at least N)t values are also listed in Supplemental Table 5. Supplemental Figure 5B displays the distribution of duplicated *CEN*s throughout the cell population [p(N)t].

Based on this simulation, we estimate that ≥ 98% of *Δdbf4/pDBF4*cells will have duplicated at least 6, 7 and 8 *CEN*s after 60, 75 and 90 min in HU, respectively. 60-90 min is the timeframe during which spindle extension occurs in *rad53* mutants treated with HU. Thus, if amphitelic attachments contribute to spindle integrity during early S phase, the number of *CEN*s duplicated by 90 min

presumably places an upper limit on the number of bioriented Ks that could be involved. 98% of the population was used as a reference since WT cells treated with HU typically exhibit a frequency of spindle extension below 2%. As forks advanced throughout the simulation, *CEN* duplication plateaued at a minimum of 13 *CEN*s in ≥ 98% of the population after 210 min. In comparison, after 60 min in HU only 84% of *Δdbf4/pdbf4-zn*cells are predicted to have duplicated at least one *CEN* (Figure7B and Supplemental Table 5). As the simulation continues, *Δdbf4/pdbf4-zn*p(at least N) increased to 2 duplicated *CEN*s in ≥ 98% of the population by 150 min and plateaued with at least 7 *CEN*s being duplicated in ≥ 98% of the cells between 270-300 min..

ORIutilization values based on normalization to maximum profile area. We performed an additional simulation where *ORI* utilization values were determined relative to the maximum replication profile *ORI*AUC (rather than maximum non-outlier *ORI*AUC). This simulation was limited to the *Δdbf4/pDBF4*dataset at 60, 75 and 90 min. In this case, we obtained estimates of at least 4, 5 and 6 *CENs* being duplicated in ≥ 98% of the population at these respective times (not shown).

Setting ORI utilization values for all 32 CEN flanking ORIs to 1. We also performed a simulation in which all 32 *CEN* flanking *ORI*s were assumed to fire in every cell after 60 min in HU, effectively limiting *CEN* duplication only by *CEN-ORI* distance and the rate of replication fork movement. In this case, ≥ 98% of *Δdbf4/pDBF4*cells were predicted to have duplicated at least 9, 10, and 12 *CEN*s after 60, 75 and 90 min in HU, and all 16 *CEN*s reached 100% duplication by the end of the simulation. If we set the relative utilization values for all 45 *CEN* proximal *ORI*s included in our simulation in WT cells to 1, and applied the ratio of *Δdbf4/pdbf4-zn* to *Δdbf4/pDBF4ORI* AUCs as described previously, *Δdbf4/pdbf4-zn*mutants were projected to display a minimum of 0, 2 and 3 *CEN*s being duplicated in ≥ 98% of the population at 60, 75 and 90 mins in HU, respectively, increasing rapidly thereafter to at least 12 *CEN*s being duplicated by 300

min (not shown). With respect to our datasets, this treatment effectively places an upper limit on the extent of *CEN* duplication that could conceivably be achieved in HU treated *Δdbf4/pdbf4-zn* cells.

Overall, based on this analysis, assignment of relative *ORI* utilization values greatly affects the extent of *CEN* duplication in our calculations. It is interesting, however, that in all cases the plateau of *CEN* duplication occurs between 180-210 min into the simulation. The timing of this plateau corresponds well with the reported transition to a Pds1-dependent mode of maintaining pre-anaphase spindle organization(Clarke *et al.*, 2001). A second notable outcome is that, compared to *Δdbf4/pDBF4*, *Δdbf4/pdbf4-zn*cells experience an initial hiatus in *CEN* duplication due to the strong reduction in utilization of *CEN* flanking *ORI*s. In the main text, we propose that this displacement in fork approach may be responsible for the ability of the p*dbf4-zn* allele to rescue *rad53-21* spindle extension in HU.

Yabuki et al, 2002 Calculations

These investigators used differential hybridization to genome microarrays to measure changes in DNA copy number between G_1 standards and HU treated samples (200 mM HU, 90 min, 26°C; Yabuki *et al.*, 2002). Thus, an advantage of this dataset is that hybridization values can be used to directly calculate p(*CEN*)t. Increases in hybridization ratios for HU treated cells were reported to be low in these experiments, and to offset false positive signals only replication peaks that appeared in each of four replicates were included in the final data set. We note that 21 of the *CEN*-flanking *ORI*s captured in their data set are identical to those in our study (compare Supplemental Table 1 with Supplemental Table 4). Where differences are observed, flanking *ORI*s in the Yabuki*et al*., 2002 data are found at a greater distance from the *CEN*. As a first step in evaluating their data, the hybridization ratios listed in Table S1 of Yabuki*et al*., 2002 were converted to DNA copy number using equation 3:

3. $y = 0.5x + 1$

where (y) is relative DNA copy number and (x) is the ratio from Table S1 in their supplementary data. The maximum change in DNA copy number we calculated from this data was 1.28 (ARS1021), in agreement with Figure 3 of their report. Using the change in DNA copy number at *CEN* positions as p(*CEN*)90 values, and applying equations 1 and 2, we calculate that only 53% of the cell population is predicted to have duplicated at least one *CEN* at the 90 min sampling time. This low estimate may reflect technical limitations of the experiment. To try and accommodate this, we determined the proportionality constant necessary to transform the ARS1021 hybridization ratio to a DNA copy number of 2.0, effectively setting the relative utilization of this *ORI* to 1. In this case, the amplitudes of all 126 *ORI*s identified in in their study fit a normal distribution; there were no outliers. After multiplying each hybridization ratio by the proportionality constant, the adjusted ratios were converted to relative copy number according to equation 3. For the set of 32 *CEN* flanking *ORI*s, this transformation increased the average *ORI* utilization score from 0.12 based on the raw data to 0.44 (Supplemental Table 4).

As a second transformation, we expanded the base of the elevated replication profiles to retain the contours of the original profile. To do this, the peak to base ratio of the original profile was determined, and this ratio was used to proportionally expand x-axis bp values in both directions from the *ORI* center. After applying this transformation, the average maximum extent of replication fork advance for the 64 fork tracks emanating from *CEN* flanking *ORI*s increased from 13,000 to 16,600 bp. p(*CEN*)90 values were again obtained directly from the transformed replication profiles. After solving for equations 1 and 2, our calculations indicate that ≥ 98% of the cell population is expected to have duplicated at least 4 *CEN*s after 90 min in HU (Supplemental Table 4). Thus, combining the results of the two data sets, our statistical modeling suggests that after 90 min following G_1 release into HU-a point at which a shortbipolar S phase spindle is already formed-≥ 98% of WT cells will have duplicated a minimum of 4-8 *CEN*s.

SUPPLEMENTAL REFERENCES

Allen, JB, Zhou, Z, Siede, W, Friedberg, EC, and Elledge, SJ (1994). The SAD1/RAD53 protein kinase controls multiple checkpoints and DNA damage-induced transcription in yeast. Genes Dev 8, 2401–2415.

Bachant, J, Alcasabas, A, Blat, Y, Kleckner, N, and Elledge, SJ (2002). The SUMO-1 isopeptidase Smt4 is linked to centromeric cohesion through SUMO-1 modification of DNA topoisomerase II. Mol Cell 9, 1169–1182.

Bachant, J, Jessen, SR, Kavanaugh, SE, and Fielding, CS (2005). The yeast S phase checkpoint enables replicating chromosomes to bi-orient and restrain spindle extension during S phase distress. J Cell Biol 168, 999–1012.

Bouck, DC, and Bloom, K (2007). Pericentric Chromatin is an Elastic Component of the Mitotic Spindle. Curr Biol CB 17, 741–748.

Clarke, DJ, Segal, M, Jensen, S, and Reed, SI (2001). Mec1p regulates Pds1p levels in S phase: complex coordination of DNA replication and mitosis. Nat Cell Biol 3, 619–627.

Crabbé, L, Thomas, A, Pantesco, V, De Vos, J, Pasero, P, and Lengronne, A (2010). Analysis of replication profiles reveals key role of RFC-Ctf18 in yeast replication stress response. Nat Struct Mol Biol 17, 1391–1397.

Feng, W, Bachant, J, Collingwood, D, Raghuraman, MK, and Brewer, BJ (2009). Centromere Replication Timing Determines Different Forms of Genomic Instability in Saccharomyces cerevisiae Checkpoint Mutants During Replication Stress. Genetics 183, 1249–1260.

Feng, W, Collingwood, D, Boeck, ME, Fox, LA, Alvino, GM, Fangman, WL, Raghuraman, MK, and Brewer, BJ (2006). Genomic mapping of single-stranded DNA in hydroxyurea-challenged yeasts identifies origins of replication. Nat Cell Biol 8, 148–155.

Friedman, KL, Brewer, BJ, and Fangman, WL (1997). Replication profile of Saccharomyces cerevisiae chromosome VI. Genes Cells Devoted Mol Cell Mech 2, 667–678.

Gardner, MK, Pearson, CG, Sprague, BL, Zarzar, TR, Bloom, K, Salmon, ED, and Odde, DJ (2005). Tension-dependent regulation of microtubule dynamics at kinetochores can explain metaphase congression in yeast. Mol Biol Cell 16, 3764–3775.

Goh, PY, and Kilmartin, JV (1993). NDC10: a gene involved in chromosome segregation in Saccharomyces cerevisiae. J Cell Biol 121, 503–512.

Goshima, G, Saitoh, S, and Yanagida, M (1999). Proper metaphase spindle length is determined by centromere proteins Mis12 and Mis6 required for faithful chromosome segregation. Genes Dev 13, 1664–1677.

Goshima, G, and Yanagida, M (2000). Establishing biorientation occurs with precocious separation of the sister kinetochores, but not the arms, in the early spindle of budding yeast. Cell 100, 619–633.

He, X, Asthana, S, and Sorger, PK (2000). Transient sister chromatid separation and elastic deformation of chromosomes during mitosis in budding yeast. Cell 101, 763–775.

Huang, M, Zhou, Z, and Elledge, SJ (1998). The DNA replication and damage checkpoint pathways induce transcription by inhibition of the Crt1 repressor. Cell 94, 595–605.

Jones, MH, Bachant, JB, Castillo, AR, Giddings, TH, and Winey, M (1999). Yeast Dam1p Is Required to Maintain Spindle Integrity during Mitosis and Interacts with the Mps1p Kinase. Mol Biol Cell 10, 2377–2391.

Khalil, A-M, Julius, JA, and Bachant, J (2007). One step construction of PCR mutagenized libraries for genetic analysis by recombination cloning. Nucleic Acids Res 35, e104.

Krishnan, V, Nirantar, S, Crasta, K, Cheng, AYH, and Surana, U (2004). DNA replication checkpoint prevents precocious chromosome segregation by regulating spindle behavior. Mol Cell 16, 687–700.

Lawrimore, J, Aicher, JK, Hahn, P, Fulp, A, Kompa, B, Vicci, L, Falvo, M, Taylor, RM, and Bloom, K (2016). ChromoShake: a chromosome dynamics simulator reveals that chromatin loops stiffen centromeric chromatin. Mol Biol Cell 27, 153–166.

Liu, H, Liang, F, Jin, F, and Wang, Y (2008). The coordination of centromere replication, spindle formation, and kinetochore-microtubule interaction in budding yeast. PLoS Genet 4, e1000262.

Lopes, M, Cotta-Ramusino, C, Pellicioli, A, Liberi, G, Plevani, P, Muzi-Falconi, M, Newlon, CS, and Foiani, M (2001). The DNA replication checkpoint response stabilizes stalled replication forks. Nature 412, 557–561.

Lopez-Mosqueda, J, Maas, NL, Jonsson, ZO, DeFazio Eli, LG, Wohlschlegel, J, and Toczyski, DP (2010). Damage-Induced Phosphorylation of Sld3 is Important to Block Late Origin Firing. Nature 467, 479–483.

Luo, H, Li, J, Eshaghi, M, Liu, J, and Karuturi, RKM (2010). Genome-wide estimation of firing efficiencies of origins of DNA replication from time-course copy number variation data. BMC Bioinformatics 11, 247.

Ma, L, McQueen, J, Cuschieri, L, Vogel, J, and Measday, V (2007). Spc24 and Stu2 promote spindle integrity when DNA replication is stalled. Mol Biol Cell 18, 2805–2816.

Nannas, NJ, O'Toole, ET, Winey, M, and Murray, AW (2014). Chromosomal attachments set length and microtubule number in the Saccharomyces cerevisiae mitotic spindle. Mol Biol Cell 25, 4034–4048.

Ortiz, J, Stemmann, O, Rank, S, and Lechner, J (1999). A putative protein complex consisting of Ctf19, Mcm21, and Okp1 represents a missing link in the budding yeast kinetochore. Genes Dev 13, 1140–1155.

Poli, J, Tsaponina, O, Crabbé, L, Keszthelyi, A, Pantesco, V, Chabes, A, Lengronne, A, and Pasero, P (2012). dNTP pools determine fork progression and origin usage under replication stress. EMBO J 31, 883–894.

Raghuraman, MK, Winzeler, EA, Collingwood, D, Hunt, S, Wodicka, L, Conway, A, Lockhart, DJ, Davis, RW, Brewer, BJ, and Fangman, WL (2001). Replication dynamics of the yeast genome. Science 294, 115–121.

Romao, M, Tanaka, K, Sibarita, J-B, Ly-Hartig, NTB, Tanaka, TU, and Antony, C (2008). Three-dimensional electron microscopy analysis of ndc10-1 mutant reveals an aberrant organization of the mitotic spindle and spindle pole body defects in Saccharomyces cerevisiae. J Struct Biol 163, 18–28.

Santocanale, C, and Diffley, JF (1998). A Mec1- and Rad53-dependent checkpoint controls late-firing origins of DNA replication. Nature 395, 615–618.

Severin, F, Hyman, AA, and Piatti, S (2001). Correct spindle elongation at the metaphase/anaphase transition is an APC-dependent event in budding yeast. J Cell Biol 155, 711–718.

Skibbens, RV, Corson, LB, Koshland, D, and Hieter, P (1999). Ctf7p is essential for sister chromatid cohesion and links mitotic chromosome structure to the DNA replication machinery. Genes Dev 13, 307–319.

Stephens, AD et al. (2013). Pericentric chromatin loops function as a nonlinear spring in mitotic force balance. J Cell Biol 200, 757–772.

Stephens, AD, Haase, J, Vicci, L, Taylor, RM 2nd, and Bloom, K (2011). Cohesin, condensin, and the intramolecular centromere loop together generate the mitotic chromatin spring. J Cell Biol 193, 1167–1180.

Tanaka, T, Fuchs, J, Loidl, J, and Nasmyth, K (2000). Cohesin ensures bipolar attachment of microtubules to sister centromeres and resists their precocious separation. Nat Cell Biol 2, 492–499.

Warsi, TH, Navarro, MS, and Bachant, J (2008). DNA topoisomerase II is a determinant of the tensile properties of yeast centromeric chromatin and the tension checkpoint. Mol Biol Cell 19, 4421–4433.

Yabuki, N, Terashima, H, and Kitada, K (2002). Mapping of early firing origins on a replication profile of budding yeast. Genes Cells Devoted Mol Cell Mech 7, 781–789.

Yamashita, M, Hori, Y, Shinomiya, T, Obuse, C, Tsurimoto, T, Yoshikawa, H, and Shirahige, K (1997). The efficiency and timing of initiation of replication of multiple replicons of Saccharomyces cerevisiae chromosome VI. Genes Cells Devoted Mol Cell Mech 2, 655–665.

Yeh, E, Haase, J, Paliulis, LV, Joglekar, A, Bond, L, Bouck, D, Salmon, ED, and Bloom, KS (2008). Pericentric chromatin is organized into an intramolecular loop in mitosis. Curr Biol CB 18, 81–90.

Supplemental Table 1. *CEN* flanking *ORI*s and p(*CEN*)t values in HU treated *Δdbf4/pDBF4*cells.

	Left flanking *ORI*			Right flanking *ORI*			p(*CEN*)t[3]		
CEN	*ORI*	Δ[1]	Rel E[2]	*ORI*	Δ[1]	Rel E[2]	60 min	75 min	90 min
CEN1	ARS108	-3966	0.44	ARS109	8494	0.35	0.39	0.46	0.52
CEN2	ARS208	-422	0.69	ARS209	16776	0.69	0.69	0.69	0.69
CEN3	ARS307	-5550	0.68	ARS308	187	0.50	0.69	0.74	0.80
CEN4	ARS415	-14621	0.27	ARS416	12829	0.06	0.00	0.01	0.02
CEN5	ARS510	-6287	0.69	ARS511	21737	0.67	0.31	0.43	0.53
CEN6	ARS605	-12534	0.24	ARS606	19106	1.00	0.01	0.02	0.03
CEN7	ARS719	-11936	0.19	ARS720	11874	0.42	0.03	0.06	0.10
CEN8	ARS805.5	-10699	0.39	ARS805.7	5885	0.27	0.15	0.22	0.30
CEN9	ARS919	-13677	0.98	ARS920	1591	0.98	0.97	0.98	0.98
CEN10	ARS1014	-19049	0.49	ARS1015	6395	0.31	0.12	0.17	0.22
CEN11	ARS1113	-22887	0.05	ARS1114	7950	0.67	0.17	0.24	0.33
CEN12	ARS1207	-12213	0.53	ARS1209	5879	0.60	0.28	0.40	0.52
CEN13	ARS1309	-4911	1.00	ARS1310	18803	0.92	0.65	0.81	0.93
CEN14	ARS1424	-19253	0.93	ARS1426	6968	0.53	0.18	0.24	0.33
CEN15	ARS1512	-17001	0.24	ARS1513	10815	0.73	0.07	0.11	0.16
CEN16	XVI-553	-2670	0.41	ARS1622	7895	0.55	0.46	0.52	0.57

1. Distance between midpoints of *CEN* and *ORI* in bp.

2. Relative *ORI* efficiency (REL E) values were determined by normalizing the *ORI*AUC for each *ORI* to the largest *ORI*AUC value in the dataset that was not a statistical outlier. *ORI*s with Rel E values ≥ 1 were set to 1.0

3. p(*CEN*)t is the probability of a *CEN* being duplicated by flanking or proximal *ORI*s at the indicated times following G_1 release into 200 mM HU at 30°C.

Supplemental Table 2. *CEN* flanking *ORI*s and p(*CEN*)t values in HU treated *Δdbf4/pdbf4-zn*cells.

	Left flanking *ORI*				Right flanking *ORI*				p(*CEN*)t[4]		
CEN	*ORI*	Δ[1]	Ratio[2]	Rel E[3]	*ORI*	Δ[1]	Ratio[2]	Rel E[3]	60	75	90
CEN1	ARS108	-3966	0.39	0.17	ARS109	8494	0.55	0.19	0.17	0.20	0.24
CEN2	ARS208	-422	0.42	0.29	ARS209	16776	0.42	0.29	0.29	0.29	0.29
CEN3	ARS307	-5550	0.26	0.18	ARS308	187	0.17	0.45	0.50	0.52	0.53
CEN4	ARS415	-14621	0.45	0.12	ARS416	12829	0.88	0.05	0.00	0.01	0.01
CEN5	ARS510	-6287	0.23	0.15	ARS511	21737	0.48	0.32	0.07	0.10	0.12
CEN6	ARS605	-12534	0.33	0.08	ARS606	19106	0.67	0.67	0.00	0.01	0.01
CEN7	ARS719	-11936	0.54	0.10	ARS720	11874	0.17	0.07	0.01	0.02	0.03
CEN8	ARS805.5	-10699	0.05	0.02	ARS805.7	5885	0.15	0.04	0.02	0.03	0.04
CEN9	ARS919	-13677	0.13	0.13	ARS920	1591	0.13	0.13	0.13	0.13	0.14
CEN10	ARS1014	-19049	0.66	0.33	ARS1015	6395	0.33	0.10	0.04	0.05	0.07
CEN11	ARS1113	-22887	0.29	0.01	ARS1114	7950	0.35	0.23	0.06	0.08	0.11
CEN12	ARS1207	-12213	0.03	0.02	ARS1209	5879	0.02	0.01	0.01	0.01	0.01
CEN13	ARS1309	-4911	0.19	0.19	ARS1310	18803	0.88	0.81	0.13	0.16	0.18
CEN14	ARS1424	-19253	0.44	0.41	ARS1426	6968	0.09	0.05	0.02	0.02	0.03
CEN15	ARS1512	-17001	0.50	0.12	ARS1513	10815	0.37	0.27	0.02	0.04	0.06
CEN16	XVI-553	-2670	0.18	0.07	ARS1622	7895	0.15	0.09	0.09	0.10	0.11

1. Distance between midpoints of *CEN* and *ORI* in bp.
2. Ratio of *ORI*AUCs; *dbf4-Δ*/p*db4-zn* G_1/S *ORI*AUC divided by *dbf4-Δ*/p*DBF4* G_1/S *ORI*AUC.
3. Relative *ORI* efficiency values for *dbf4-Δ*/p*db4-zn* cells were determined by multiplying *Δdbf4/pDBF4*Rel E values for each *ORI*(Supplemental Table 1) by the corresponding *ORI*AUC ratio for*dbf4-Δ*/p*db4-zn.*
4. p(*CEN*)t is the probability of a *CEN* being duplicated by flanking or proximal *ORI*s at the indicated times following G_1 release into 200 mM HU at 30°C.

Supplemental Table 3. Differentially up- and down-regulated *ORI*s in HU treated *Δdbf4/pdbf4-zn*cells.

Xsome[1]	Coord[2]	ARS	INC or DEC[3]	Δ to *CEN*[4]
1	13740	ARS107.5	DEC	14124
1[5]	14717	ARS108	DEC	3966
1	17628	ARS110	DEC	24757
2	23772	ARS208	DEC	422
3	39432	ARS305	DEC	75011
3	74567	ARS306	DEC	39876
3	10903	ARS307	DEC	5550
3	11464	ARS308	DEC	187
4	43522	ARS415	DEC	14621
4	91395	ARS428	DEC	464142
5	94098	ARS508	DEC	57948
5	14561	ARS510	DEC	6287
5	17375	ARS511	DEC	21737
6	19948	ARS607	DEC	50869
7	50884	ARS720	DEC	11874
7	888475	ARS731.5	DEC	391496
8	11150	ARS805.7	DEC	5885
9	341975	ARS919	DEC	13677
9	35725	ARS920	DEC	1591
10	41701	ARS1014	DEC	19049
10	44243	ARS1015	DEC	6395
10	612759	ARS1019	DEC	176393
11	447775	ARS1114	DEC	7950
11	456825	ARS1114.5	DEC	16637
12	140000	ARS1207	DEC	12213
12	156765	ARS1209	DEC	5879
13	263179	ARS1309	DEC	4911
14	609582	ARS1424	DEC	19253
15	277654	ARS1510.5	DEC	48990
15	337404	ARS1513	DEC	10815
16	559633	XVI-560	DEC	3618
16	563942	ARS1622	DEC	7895
2	486785	ARS216	INC	248520
4	1057952	ARS431	INC	608186
7	659932	ARS727	INC	162953
9	247690	ARS914	INC	107998

10	67708	ARS1005	INC	368658
10	654189	ARS1020	INC	217823
11	98449	ARS1104.5	INC	341739
11	153054	ARS1106	INC	287134
11	329447	ARS1109	INC	110741
11	388755	ARS1112	INC	51433
11	516778	ARS1116	INC	76590
13	371099	ARS1312	INC	103009
15	85320	ARS1508	INC	241324
15	489887	ARS1514	INC	163244
15	874312	ARS1526	INC	547669
16	289594	ARS1614	INC	266422
16	384660	ARS1618	INC	171355
16	418246	ARS1619	INC	137770
16	819273	ARS1627	INC	263258

1. Chromosome.

2. Chromosome coordinate for *ARS* element midpoint (bp).

3. The difference between *Δdbf4/pDBF4* and *Δdbf4/pdbf4-zn* S/G_1 ssDNA amplitudes was calculated at each array position. Genome regions that were either decreased (DEC; blue, Figure 6C) or increased (INC; green, Figure 6C) by three standard deviations from the median difference were identified and centered around corresponding *ARS* elements. Only those *ORI*s that were differentially altered on both sides of the *ORI* peak were included. These *ORI*s define the set considered to be most significantly increased or decreased in HU treated *Δdbf4/pdbf4-zn* mutants (200 mM HU, 60 min post G_1 release, 30°C).

4. Distance from *ARS* element to corresponding *CEN* (bp).

5. Rows with *CEN* flanking *ORI*s are highlighted in grey.

Supplemental Table 4. *CEN* flanking *ORI*s and p(*CEN*)t values in HU treated WT cells based on data from Yabuki et al., 2002

	Left flanking *ORI*			Right flanking *ORI*			p(*CEN*)90[3]
CEN	*ORI*	Δ[1]	Rel E[2]	*ORI*	Δ[1]	Rel E[2]	90 min
CEN1	ARS107	-27038	0.22	ARS110	24769.5	0.24	0.00
CEN2	ARS208	-422	0.40	ARS210	20750.5	0.63	0.38
CEN3	ARS307	-5550	0.61	ARS309	17638.5	0.23	0.44
CEN4	ARS415	-14621	0.63	ARS416	12828.5	0.40	0.14
CEN5	ARS510	-6287	0.60	ARS511	21737	0.60	0.42
CEN6	ARS605	-12534	0.26	ARS606	19106	0.59	0.07
CEN7	ARS719	-11936	0.49	ARS720	11874	0.57	0.14
CEN8	ARS805	-41311	0.22	ARS806	10656	0.38	0.13
CEN9	ARS919	-13677	0.25	ARS920	1591	0.31	0.29
CEN10	ARS1014	-19049	0.78	ARS1015	6395	0.31	0.20
CEN11	ARS1109	-110382	0.30	ARS1114	7950	0.71	0.39
CEN12	ARS1206	-59348	0.33	ARS1209	5879	0.33	0.12
CEN13	ARS1309	-4911	0.48	ARS1310	18803	0.51	0.40
CEN14	ARS1424	-19253	0.55	ARS1426	6968	0.22	0.07
CEN15	ARS1511	-48989	0.80	ARS1513	10815	0.51	0.11
CEN16	ARS1621	-44301	0.21	XVI-560	3635	0.33	0.33

1. Distance between midpoints of *CEN* and *ORI* in bp.

2. Relative *ORI* efficiency values determined by based on normalizing the hybridization value for each *ORI* to the largest ORI hybridization value in the Yabuki*et al.*, 2002 dataset.

3. p(*CEN*)90 is the probability of a *CEN* being duplicated by flanking *ORI*s after 90 min following G_1 release into 200 mM HU at 26°C.

Supplemental Table 5. Fraction of cells with a minimum number of duplicated *CEN*s in HU.

	p(at least N)t, WT 30°[1]			p(at least N)t, *dbf4-zn* 30°			p(at least N)90 WT, 26°[2]
N	60 min	75 min	90 min	60 min	75 min	90 min	90 min
1	1.00	1.00	1.00	0.84	0.88	0.91	1.00
2	1.00	1.00	1.00	0.65	0.74	0.83	1.00
3	1.00	1.00	1.00	0.30	0.43	0.58	1.00
4	1.00	1.00	1.00	0.08	0.14	0.24	0.98
5	1.00	1.00	1.00	0.01	0.03	0.06	0.86
6	0.98	1.00	1.00	0.00	0.00	0.01	0.50
7	0.70	0.99	1.00	0.00	0.00	0.00	0.17
8	0.24	0.80	1.00	0.00	0.00	0.00	0.04
9	0.04	0.30	0.84	0.00	0.00	0.00	0.01
10	0.01	0.06	0.32	0.00	0.00	0.00	0.00
11	0.00	0.01	0.06	0.00	0.00	0.00	0.00
12	0.00	0.00	0.01	0.00	0.00	0.00	0.00
13	0.00	0.00	0.00	0.00	0.00	0.00	0.00
14	0.00	0.00	0.00	0.00	0.00	0.00	0.00
15	0.00	0.00	0.00	0.00	0.00	0.00	0.00
16	0.00	0.00	0.00	0.00	0.00	0.00	0.00

1. Shaded entries represent cases where ≥ 98% of the population will have, at a minimum, the indicated number of duplicated *CEN*s. WT is genotype *dbf4-Δ/pDBF4*, *dbf4-zn* is *dbf4-Δ/pdbf4-zn.*

2. Data from Yabuki et al., 2002.

Supplemental Table 6. Yeast strains used in this study

Strain	Genotype[1]	Source[2]
CRY1	*MATa his3-11,15 leu2-3,112 trp1-1 ura3-1 ade2-1 can1-100*[a]	(Bachant *et al.*, 2005)
AY201	*MATa mec1-21 HIS3*	This study
DES956	*MATa cdc7-1*	This study
DES960	*MATa cdc7-1 rad53-21*	This study
JBY546	*MATa mad2-Δ::URA3*	This study
JBY927	*MATa dbf4-1 mec1-21*	This study
JBY997	*MATa dbf4-1 LEU2*	This study
JBY999	*MATa dbf4-1*	This study
JBY1002	*MATa dbf4-1 rad53-21*	This study
JBY1129	*MATa trp1-1::SPC42-GFP-TRP1*	(Bachant *et al.*, 2005)
JBY1274	*MATa rad53-21 trp1-1::SPC42-GFP-TRP1*	(Huang *et al.*, 1998)
JBY1285	*MATa trp1-1::SPC42-GFP-TRP1 [pCEN ARS HIS3] [pμm URA3]*	This study
JBY1286	*MATa trp1-1::SPC42-GFP-TRP1 [pCEN ARS HIS3 GAL-RAD53] [p2μm URA3]*	This study

JBY1287	*MATa trp1-1::SPC42-GFP-TRP1 [pCEN ARS HIS3] [pμm URA3 GAL-DBF4]*	This study
JBY1288	*MATa trp1-1::SPC42-GFP-TRP1 [pCEN ARS HIS3] [pμm URA3 GAL-DBF4] [p2□m URA3 GAL-DBF4]*	This study
JBY1392	*MATa dbf4-1 trp1-1::SPC42-GFP-TRP1 LEU2*	This study
JBY2246	*MATa exo1-Δ::kanMX trp1-1::SPC42-GFP-TRP1*	This study
JBY2250	*MATa ctf19-Δ::kanMX trp1-1::SPC42-GFP-TRP1*	This study
JBY2251	*MATa ctf19-Δ::kanMX rad53-21 trp1-1::SPC42-GFP-TRP1*	This study
JBY2252	*MATa MTW1-GFP-LEU2*	This study
JBY2253	*MATa rad53-21 MTW1-GFP-LEU2 MIF2-myc18-HIS3*	This study
JBY2264	*MATa exo1-Δ::kanMX rad53-21 MTW1-GFP-LEU2 MIF2-myc18-HIS3*	This study
JBY2271	*MATa trp1-1::SPC42-GFP-TRP1 II-851646::LacO8-LEU2 IX-381390::LacO8-kanMX X-395744::LacO8-ADE2 XIII-115673::LacO8-URA3*	This study
JBY2273	*MATa rad53-21 trp1-1::SPC42-GFP-TRP1 II-851646::LacO8-LEU2 IX-381390::LacO8-kanMX X-395744::LacO8-ADE2 XIII-115673::LacO8-URA3 (4X-LATE-AK)*	This study
JBY2274	*MATa rad53-21 trp1-1::SPC42-GFP-TRP1 II-851646::LacO8-LEU2 IX-381390::LacO8-kanMX X-395744::LacO8-ADE2 XIII-115673::LacO8-URA3 (4X-LATE-AK)*	This study

JBY2275	*MATa rad53-21 trp1-1::SPC42-GFP-TRP1 II-851646::LacO8-LEU2 IX-381390::LacO8-kanMX X-395744::LacO8-ADE2 XIII-115673::LacO8-URA3 (4X-LATE-AK)*	This study
JBY2283	*MATa IX-353803::LacO256-LEU2 his3-11,15::LacI-GFP-HIS3 (CEN9-GFP)*	This study
JBY2289	*MATa IX-381390::LacO256-kanMX-LEU2 his3-11,15::LacI-GFP-HIS3 (LATE9-GFP)*	This study
JBY2290	*MATa rad53-21 IX-381390::LacO256-kanMX-LEU2 his3-11,15::LacI-GFP-HIS3 (LATE9-GFP)*	This study
JBY2291	*MATa X-395744::LacO256-ADE2-LEU2 his3-11,15::LacI-GFP-HIS3 (LATE10-GFP)*	This study
JBY2293	*MATa rad53-21 X-395744::LacO256-ADE2-LEU2 his3-11,15::LacI-GFP-HIS3 (LATE10-GFP)*	This study
JBY2295	*MATa rad53-21 IX-353803::LacO256-LEU2 his3-11,15::LacI-GFP-HIS3 (CEN9-GFP)*	This study
JBY2296	*MATa rad53-21 II-240817::LacO256-LEU2 XIII-115673::LacO8-URA3 his3-11,15::LacI-GFP-HIS3 (CEN2-GFP)*	This study
JBY2297	*MATa X-438358::LacO256-LEU2 his3-11,15::LacI-GFP-HIS3 (CEN10-GFP)*	This study
JBY2298	*MATa rad53-21 X-438358::LacO256-LEU2 his3-11,15::LacI-GFP-HIS3 (CEN10-GFP)*	This study
JBY2299	*MATa exo1-Δ::kanMX rad53-21 IX-353803::LacO256-LEU2 his3-11,15::LacI-GFP-HIS3 (CEN9-GFP)*	This study

JBY2301	*MATa exo1-Δ::kanMX rad53-21 X-438358::LacO256-LEU2 his3-11,15::LacI-GFP-HIS3 (CEN10-GFP)*	This study
JBY2303	*MATa exo1-Δ::kanMX rad53-21 trp1-1::SPC42-GFP-TRP1*	This study
JBY2323	*MATa dbf4-1 ura3-1::GFP-TUB1-URA3*	This study
JBY2324	*MATa dbf4-Δ::kanMX::dbf4-zn-URA3 ura3-1::GFP-TUB1-URA3*	This study
JBY2327	*MATa mcm21-Δ::kanMX trp1-1::SPC42-GFP-TRP1*	This study
JBY2330	*MATa rad53-21 mcm21-Δ::kanMX trp1-1::SPC42-GFP-TRP1*	This study
JBY2334	*MATa sld3-38-Hyg dbf4-Δ::kanMX-dbf4-m25-LEU2*	This study
JJY016	*MATa dbf4-1 [pCEN ARS TRP1 lox]*	This study
JJY017	*MATa dbf4-1 [pCEN ARS TRP1 lox(dbf4-C22)lox]*	This study
JJY023	*MATa dbf4-Δ::kanMX rad53-21 trp1-1::SPC42-GFP-TRP1 HIS3 [pCEN ARS URA3 lox(DBF4)lox*	This study
JJY028	*MATa dbf4-Δ::kanMX rad53-21 trp1-1::SPC42-GFP-TRP1 [pCEN ARS LEU2 lox(dbf4-C22)lox]*	This study
JJY029	*MATa dbf4-Δ::kanMX rad53-21 trp1-1::SPC42-GFP-TRP1 [pCEN ARS LEU2 lox(dbf4-D3)lox]*	This study
JJY030	*MATa dbf4-Δ::kanMX rad53-21 trp1-1::SPC42-GFP-TRP1 [pCEN ARS LEU2 lox(dbf4-D45)lox]*	This study
JJY032	*MATa dbf4-Δ::kanMX trp1-1::SPC42-GFP-TRP1 [pCEN ARS LEU2 lox(dbf4-C22)lox]*	This study

JJY033	*MATa dbf4-Δ::kanMX trp1-1::SPC42-GFP-TRP1 [pCEN ARS LEU2 lox(dbf4-D3)lox]*	This study
JJY037	*MATa dbf4-Δ::kanMX trp1-1::SPC42-GFP-TRP1 [pCEN ARS LEU2 lox(DBF4)lox]*	This study
JJY044	*MATa dbf4-Δ::kanMX [pCEN ARS LEU2 lox(dbf4-D45)lox]*	This study
JJY045	*MATa dbf4-Δ::kanMX::dbf4-zn-URA3 trp1-1::SPC42-GFP-TRP1*	This study
JJY046	*MATa dbf4-Δ::kanMX::DBF4-URA3*	This study
JJY059	*MATa dbf4-1 [pCEN ARS TRP1 lox(DBF4)lox]*	This study
JJY060	*MATa dbf4-1 [pCEN ARS TRP1 lox(dbf4-D3)lox]*	This study
JJY061	*MATa dbf4-1 [pCEN ARS TRP1 lox(dbf4-D45)lox]*	This study
JJY076	*MATa dbf4-Δ::kanMX::dbf4-zn-URA3*	This study
JJY080	*MATa dbf4-Δ::kanMX::dbf4-zn-URA3 rad9-Δ::HIS3 PDS1-myc18-LEU2*	This study
JJY102	*MATa dbf4-Δ::kanMX::dbf4-zn-URA3 mad2-Δ::URA3 trp1-1::SPC42-GFP-TRP1 PDS1-myc18-LEU2*	This study
JJY108	*MATa dbf4-Δ::kanMX trp1-1::SPC42-GFP-TRP1 [pCEN ARS URA3 lox(DBF4)lox]*	This study
JJY112	*MATa mcm2-1 rad53-21 trp1-1::SPC42-GFP-TRP1*	This study
JJY117	*MATa mcm3-1 rad53-21 trp1-1::SPC42-GFP-TRP1*	This study

JJY120	*MATa mcm5-1 rad53-21 trp1-1::SPC42-GFP-TRP1*	This study
JJY141	*MATa dun1-Δ::HIS3 sld3-38-FLAG3X-Hyg dbf4-Δ::kanMX::dbf4-m25-LEU2*	This study
JJY144	*MATa dun1-Δ::HIS3 sld3-38-FLAG3X-Hyg dbf4-Δ::kanMX::dbf4-m25-LEU2*	This study
JJY164	*MATa dbf4-1 [pCEN ARS HIS3 DBF4]*	This study
JJY165	*MATa dbf4-1 [pCEN ARS HIS3 dbf4-zn]*	This study
JJY166	*MATa dbf4-Δ::kanMX [pCEN ARS HIS3 DBF4]*	This study
JJY167	*MATa dbf4-Δ::kanMX [pCEN ARS HIS3 dbf4-zn]*	This study
JJY181	*MATa dbf4-Δ::kanMX trp1-1::SPC42-GFP-TRP1 [pCEN ARS LEU2 lox(dbf4-zn)lox]*	This study
JJY182	*MATa dbf4-Δ::kanMX rad53-21 trp1-1::SPC42-GFP-TRP1 HIS3 [pCEN ARS LEU2 lox(dbf4-zn)lox]*	This study
JJY184	*MATa dbf4-Δ::kanMX rad53-21 trp1-1::SPC42-GFP-TRP1 HIS3 [pCEN ARS LEU2 lox(DBF4)lox]*	This study
MY26	*MATa dun1-Δ::HIS3*	(Huang *et al.*, 1998)
Y301	*MATa rad53-21*	(Allen *et al.*, 1994)
YJLO155	*MATa RAD52-GFP-HIS3 sld3-38-FLAG3x-Hyg dbf4-Δ::kanMX::dbf4-m25-LEU2 his3Δ-1 leu2Δ-0 met15Δ-0 ura3Δ*	(Lopez-Mosqueda *et al.*, 2010)

YJLO156	*MATa RAD52-GFP-HIS3 sld3-38-FLAG3x-Hyg his3Δ-1 leu2Δ-0 met15Δ-0 ura3Δ*	(Lopez-Mosqueda *et al.*, 2010)
YJLO157	*MATa RAD52-GFP-HIS3 dbf4-Δ::kanMX::dbf4-m25-LEU2 his3Δ-1 leu2Δ-0 met15Δ-0 ura3Δ*	(Lopez-Mosqueda *et al.*, 2010)

1) Genetic markers as in CRY1 unless otherwise indicated; episomal genetic elements in [brackets].

2) See Supplemental References.

Supplemental Table 7. Plasmids used in this study

Name	Elements/(Description)[1]	Source[2]
pAS003	p*DBF4 loxAmp^{R}Tet^R* (recombination cloning plasmid)	(Khalil *et al.*, 2007)
pBAD5	p*CEN ARS HIS3 GAL-RAD53 Amp^R* (low copy episomal)	S. Elledge
pJBN231	p*2μm URA3 GAL-DBF4 Amp^R*(high copy episomal)	This study
pJBN316	p*II-851646::LacO8X-LEU2 Amp^R*(integrating, *LATE2-AK*)	This study
pJBN321	p*CEN ARS HIS3 ASK1-LacI* (low copy episomal)	This study
pJBN322	p*IX-381390::LacO8X-kanMX Amp^R*(integrating, *LATE9-AK*)	This study
pJBN323	p*X-395744::LacO8X-ADE2 Amp^R*(integrating, *LATE10-AK*)	This study
pJBN324	p*XIII-115673::LacO8X-URA3 Amp^R*(integrating, *LATE13-AK*)	This study
pJBN326	p*2μm LEU2 AD-dbf4(1-659) Amp^R* (two-hybrid, pACT-based)	This study
pJBN334	p*II-240817::LacO256-LEU2 Amp^R*(integrating, *CEN2-GFP*)	This study
pJBN335	p*IX-353803::LacO256-LEU2 Amp^R*(integrating, *CEN9-GFP*)	This study
pJBN336	p*X-438358::LacO256-LEU2 Amp^R*(integrating, *CEN10-GFP*)	This study
pJBN343	p*CEN ARS URA3 GFP-TUB1 Amp^R*(integrating)	This study
pJJ019	p*DBF4-URA3 Amp^R*(integrating)	This study

pJJ022	p*dbf4-zn-URA3 Amp*^{R}(integrating)	This study
pJJ029	p*CEN ARS HIS3 DBF4 Amp*^{R} (low copy episomal)	This study
pJJ030	p*CEN ARS HIS3 dbf4-zn Amp*^{R} (low copy episomal)	This study
pJJ031	p*CEN ARS LEU2 lox(dbf4-zn)loxAmp*^{R} (low copy episomal)	This study
pJJ032	p*CEN ARS LEU2 lox(DBF4)loxAmp*^{R} (low copy episomal)	This study
pCN514	p*2μm LEU2 AD-DBF4 Amp*^{R} (two-hybrid, pACT-based)	This study
pJBN516	p*2μm LEU2 AD-dbf4(Δ660-688) Amp*^{R} (two-hybrid, pACT-based)	This study
pCN518	p*2μm LEU2 AD-dbf4(Δ108-600) Amp*^{R} (two-hybrid, pACT-based)	This study
pCN519	p*2μm LEU2 AD-dbf4(1-276) Amp*^{R} (two-hybrid, pACT-based)	This study
pCN520	p*2μm LEU2 AD-dbf4(1-65) Amp*^{R} (two-hybrid, pACT-based)	This study
pAS-*CTF19*	p*2μm TRP1 DBD-CTF19 Amp*^{R} (two-hybrid, pAS-based)	(Ortiz *et al.*, 1999)

1. Only expression constructs are listed.

2) See Supplemental References.

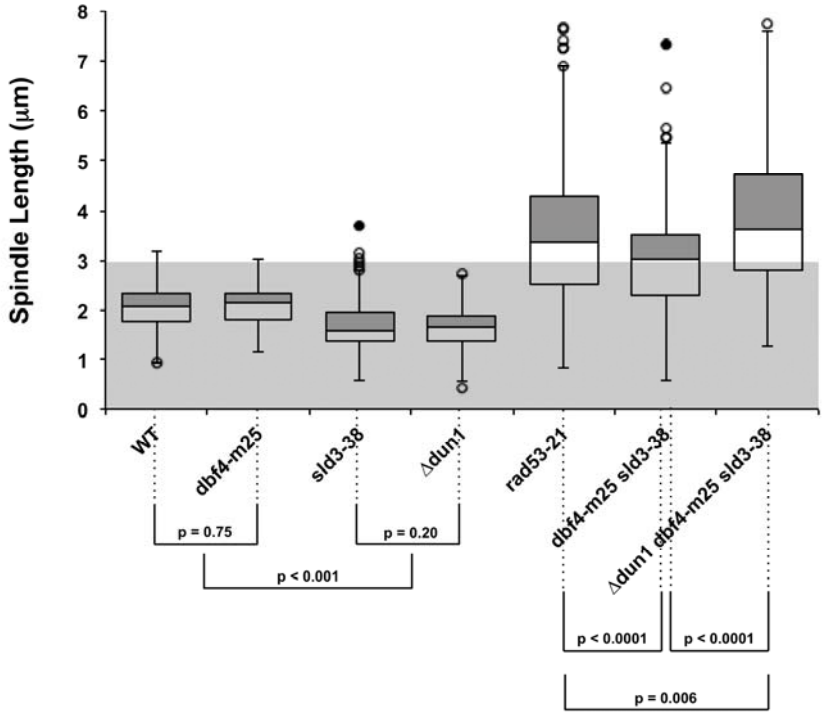

SUPPLEMENTAL FIGURE 1

Supplemental Figure 1. Spindle extension in *dun1-Δ dbf4-m25 sld3-38A* mutants. Box plots summarizing combined spindle extension data for three experiments using the strains described in the legend for Figure 3. p values (two-tailed t-test) for the indicated comparisons are shown. Simultaneously preventing expansion of dNTP pools and activating firing of checked *ORI*s engenders a distribution of extended spindles in HU that is comparable a *rad53* mutant.

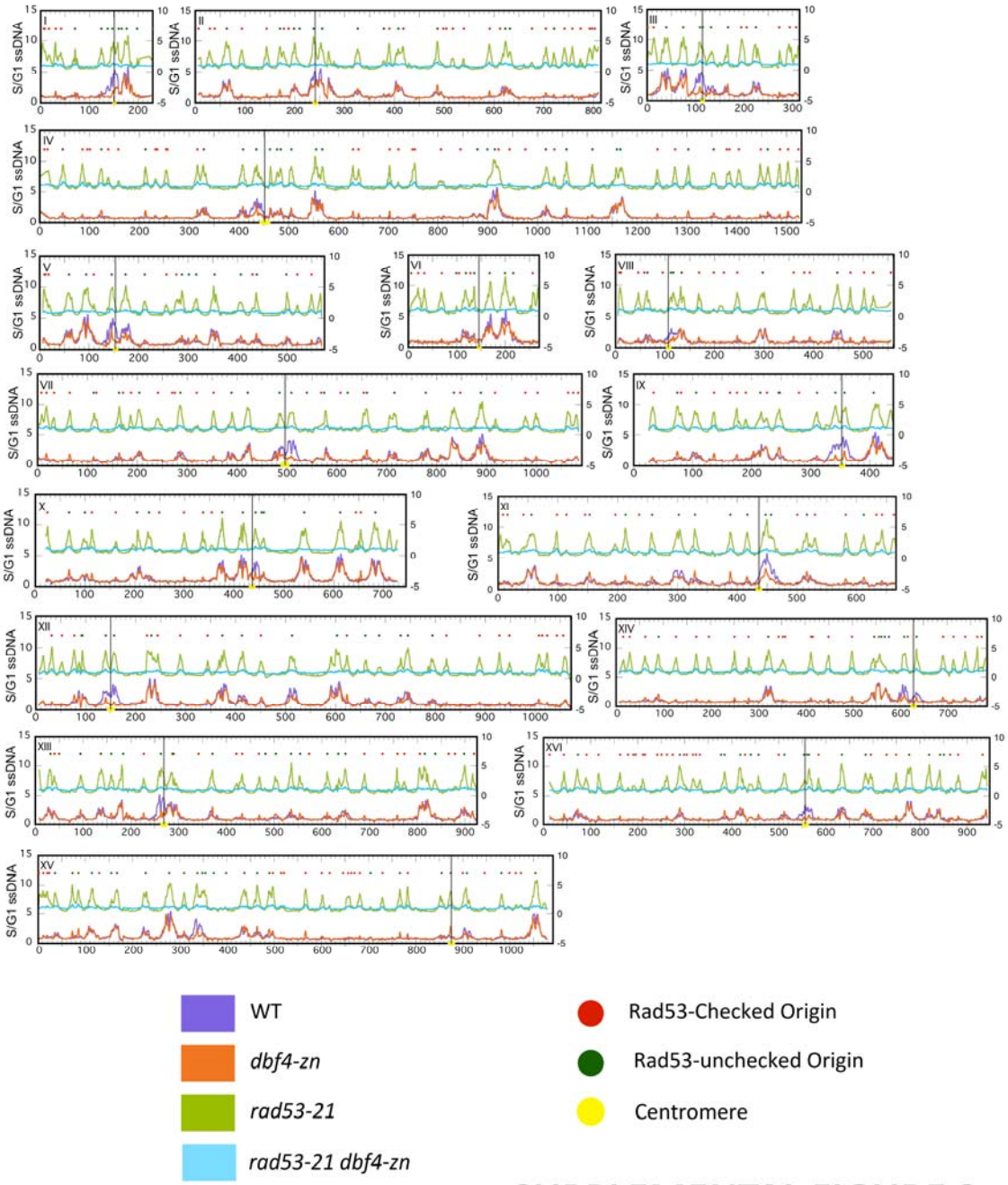

SUPPLEMENTAL FIGURE 2

Supplemental Figure 2. ssDNA replication profiles in HU. *dbf4-Δ/pDBF4*(WT on figure; JJY108), *dbf4-Δ/pdbf4-zn* (*dbf4-zn* on figure; JJY181), *rad53-21 dbf4-Δ/pDBF4*(*rad53-21* on figure; JJY023), and *rad53-21 dbf4-Δ/pdbf4-zn* (*rad53-21 dbf4-zn* on figure; JJY182) strains were arrested in G_1 or released into media containing 200 mM HU (60 min, 30°C). ssDNAs from the arrested cells were hybridized to genome microarrays. The ratio of the S to G_1 ssDNA hybridization signals at each array position was plotted to generate replication profiles for all 16 chromosomes. Positions of *CEN*s and Rad53 checked and un-checked *ORI*s are indicated.

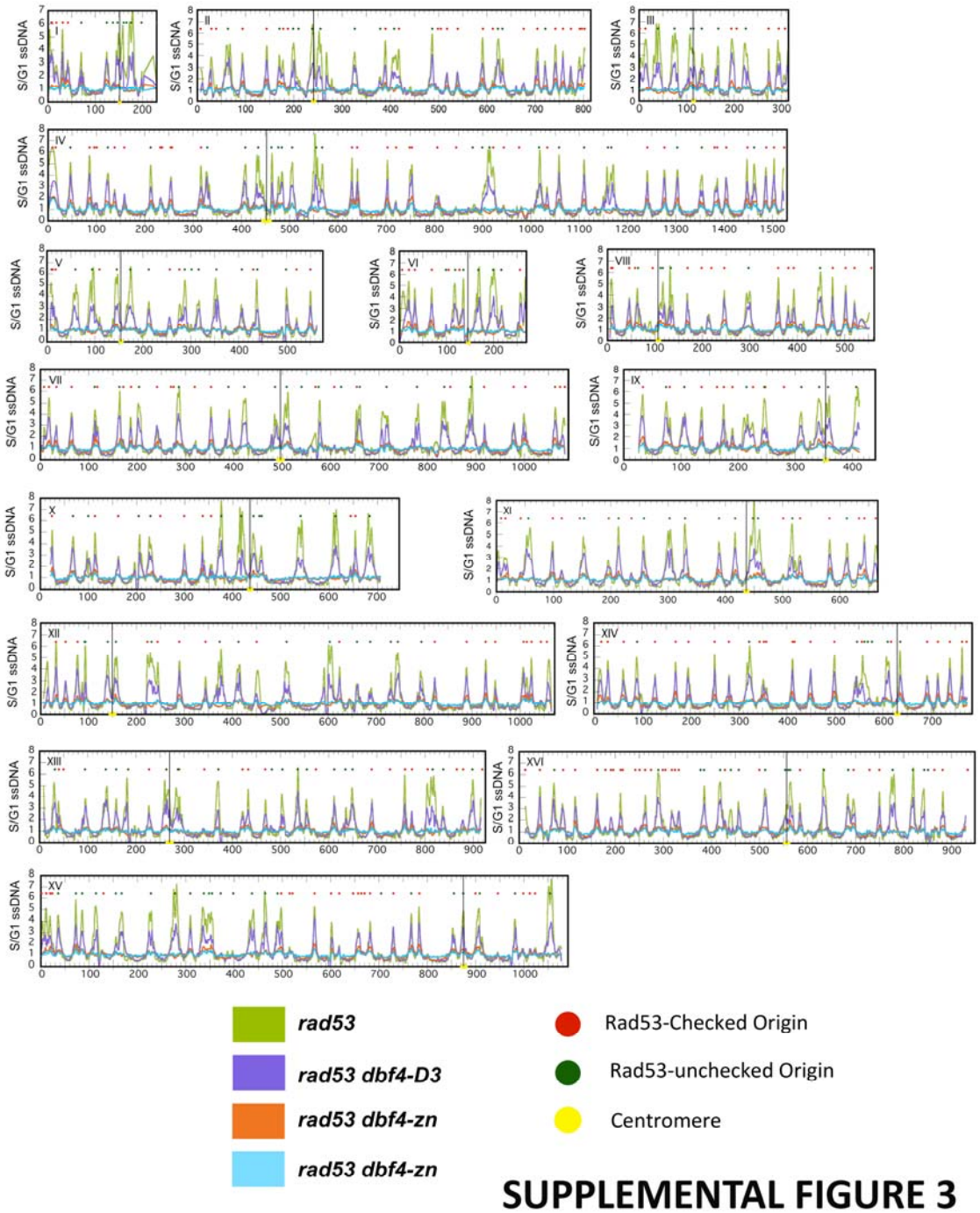

SUPPLEMENTAL FIGURE 3

Supplemental Figure 3.ssDNA replication profiles in HU. *rad53-21 dbf4-Δ/pDBF4*(*rad53* on figure; JJY023), *rad53-21 dbf4-Δ/pdbf4-D3*(*rad53dbf4-D3* on figure; JJY029), and duplicate cultures for*rad53-21 dbf4-Δ/pdbf4-zn* (*rad53dbf4-zn* on figure; JJY182) strains were arrested in G_1 or released into media containing 200 mM HU (60 min, 30°C). p*dbf4-D3* is one of the PCR mutagenized C-terminal *dbf4* alleles shown in Figure 2A. It behaves in a similar manner with respect to suppression of *rad53* spindle extension in HU compared to p*dbf4-zn* (Figure 4A and B). ssDNAs from the arrested cells were hybridized to genome microarrays, and the ratios of the S to G_1 hybridization signals were plotted to generate replication profiles for all 16 chromosomes. The *rad53-21 dbf4-Δ/pDBF4*and *rad53-21 dbf4-Δ/pdbf4-zn*datasets shown here are distinct replicates from those shown in Supplemental Figure 2. Positions of *CEN*s and Rad53 checked and un-checked *ORI*s are indicated.

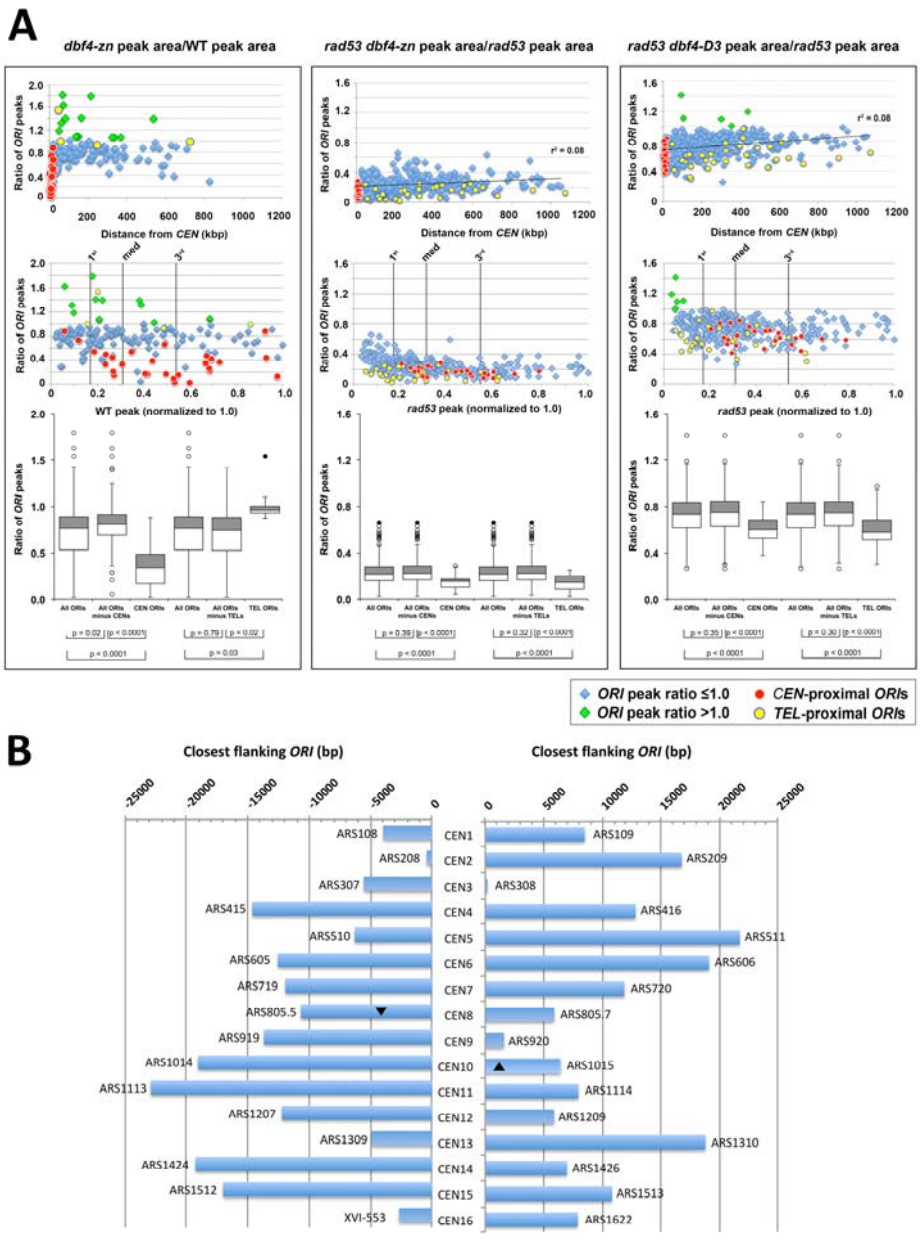

SUPPLEMENTAL FIGURE 4

Supplemental Figure 4. *ORI* utilization in *pdbf4-zn* and *rad53 pdbf4* mutants. A) As labelled on the figure, *dbf4-Δ/pDBF4*=WT; *dbf4-Δ/pdbf4-zn=dbf4-zn*, *rad53-21 dbf4-Δ/pDBF4=rad53-21, rad53-21 dbf4-Δ/pdbf4-zn=rad53-21dbf4-zn*and *rad53-21 dbf4-Δ/pdbf4-D3=rad53-21 dbf4-D3.* *ORI*AUCs were determined from replication profiles for 177*ORI*s that fire in HU treated p*dbf4-zn* and WT cells, and 403 *ORI*s that fire in HU treated *rad53-21*, *rad53-21 pdbf4-zn* and *rad53-21 pdbf4-D3* cells. Ratios of p*dbf4-zn*to WT *ORI* AUCs (ratio of *ORI* peaks on y-axis in left graphs), *rad53-21 pdbf4-zn* to *rad53-21ORI*AUCs (ratio of *ORI* peaks on y-axis in middle graphs), and *rad53-21 dbf4-D3* to *rad53-21ORI*AUCs (ratio of *ORI* peaks on y-axis in right graphs) were calculated for each *ORI*. Upper graphs. Upper graphs display the ratio of *ORI*AUCs as a function of *ORI* distance to the corresponding *CEN*. There is a pronounced reduction in *ORI* utilization in the p*dbf4-zn* mutant at *CEN*-proximal regions. Regression lines are plotted through the *rad53-21 pdbf4-zn* to *rad53-21* and *rad53-21 pdbf4-D3* to *rad53*-21 data sets (data on upper graphs is also displayed in Figure 4B). Lower graphs. Lower graphs display the ratio of *ORI*AUCsplotted as a function of relative *ORI* utilization in WT or *rad53-21* controls. Relative *ORI* utilization was calculated by normalizing all *ORI*AUCs to the maximum *ORI*AUC value in the WT or *rad53-21* data sets that was not a statistical outlier (defined as Q3 + 1.5*IQR). 1st quartile, median and 3rd quartile *ORI* values are indicated along the x-axis. *ORI*s that are up-regulated in the p*dbf4-zn* and *rad53 pdbf4-D3* data sets tend to be less efficiently utilized *ORI*s. Legend for graphs. *TELORI*s are defined as the most terminal *ORI* on each chromosome that fires in *rad53-21*. Boxplots. Distributions for p*dbf4-zn*/WT, *rad53-21 pdbf4-zn*/*rad53-21* and *rad53-21 pdbf4-D3/rad53-21ORI*AUCratios are shown, including distributions for *CEN*-flanking and *TEL*-flanking *ORI*s. Indicated statistical comparisons are two-tailed t-tests. Open circle outliers defined as (Q3 + 1.5*IQR), filled circle outliers defined as (Q3 + 3.0*IQR). *CEN* flanking *ORI*s are significantly reduced in all three *dbf4* mutant backgrounds compared to WT cells and *rad53* mutants. In *rad53 pdbf4* mutant comparisons to *rad53*, *TELORI*s are also preferentially reduced. B) Schematic of *CEN* flanking *ORI*s. The identity of the 32 *CEN*-flanking *ORI*s that fire in HU treated WT

and *rad53* cells was determined by comparing chromosomal coordinates for ssDNA peaks in our datasets with known *ORI* locations (www.yeastgenome.org, www.oridb.org). Bars in the schematic indicate distances between left- and right-flanking *ORI*s and the corresponding *CEN* (see also Supplemental Table 1). With the exception of ARS805.5, all the *CEN*-flanking *ORI*s identified have been previously characterized as firing in HU (for *CEN*8, previously reported as ARS805, 41,273 bp distant from *CEN8*). Three *CEN*-flanking *ORI*s that are closer to the *CEN* than those shown here are listed in ORIdb: V-165, a dubious *ORI* located 12,605 bp from *CEN5* (not indicated on diagram); ARS113.5, a confirmed *ORI* 4,607 bp from *CEN11* (downward arrowhead); and XIII-269, a likely *ORI* 1,015 bp from *CEN13* (upward arrowhead).

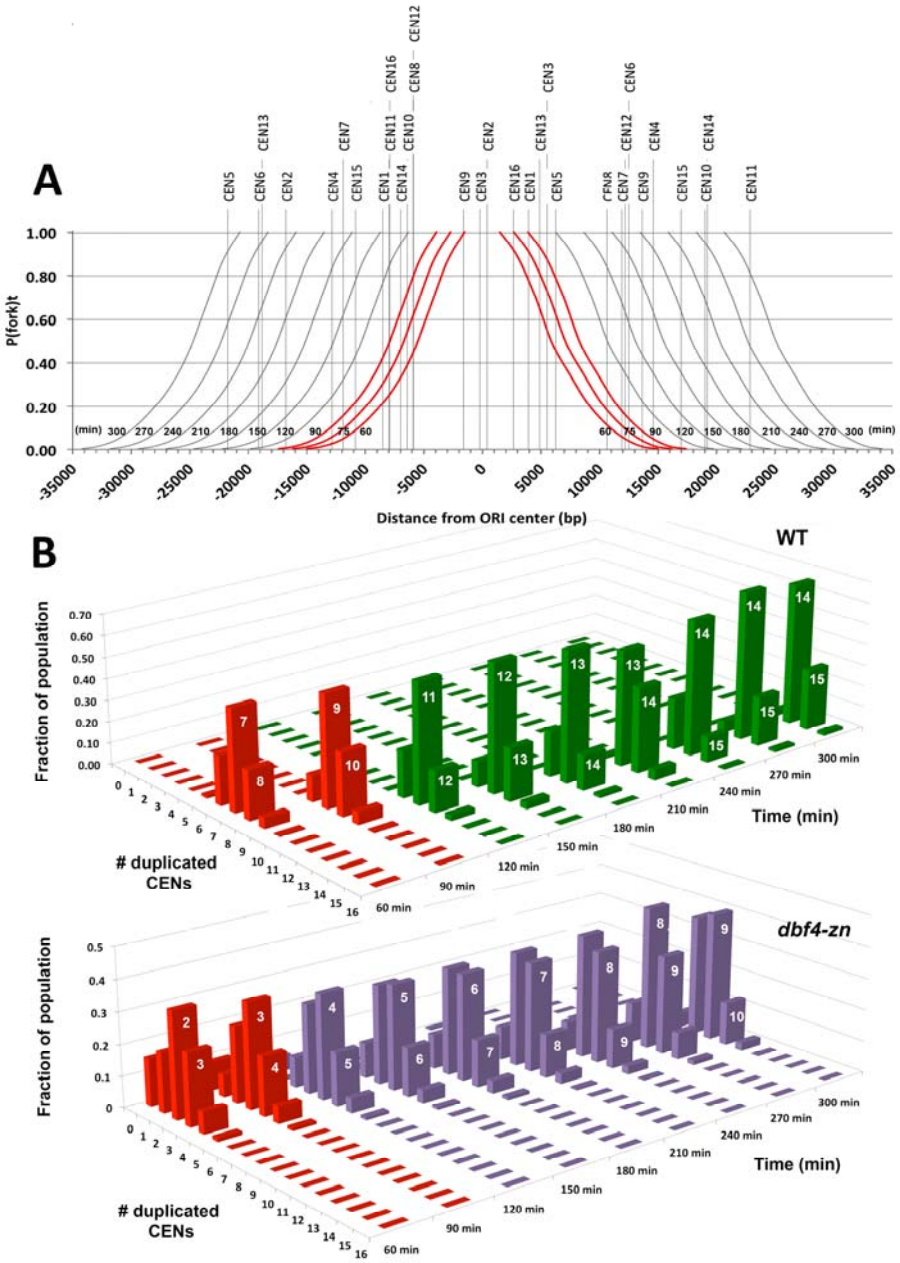

SUPPLEMENTAL FIGURE 5

Supplemental Figure 5. Analysis of *CEN* duplication in HU**.** A)As described in Supplemental Results, a first step in calculating the extent of *CEN* duplication in HU was to estimate the probability that a replication fork emanating from a *CEN*-proximal *ORI* would traverse the *CEN* after time (t) of HU exposure. These probabilities were estimated by dividing the WT (*dbf4-Δ/pDBF4*) composite replication profile shown in Figure 7A into 1000 bp intervals. The cumulative area associated with the intervals was determined, starting from the left and right edges of the profile and integrating toward the *ORI* center. The integrated area values were then expressed as a fraction of the total area encompassed by the left or right sides of the profile, yielding probability curves for fork movement in either direction. 5^{th} order polynomial equations were fitted to these probability curves ($r^2 \geq 0.999$), and the equations were advanced in both directions at a constant rate of 80 bp/min for 75 and 90 min (red curves-the time during which the spindle is formed in WT cells and p*dbf4-zn* mutants and spindle extension is observed in HU treated *rad53* mutants), and at 30 min intervals thereafter for a total of 300 min of simulated HU treatment (grey curves). Drop lines indicate the distances separating left and right flanking *ORI*s from the *CEN*. Intersections between the drop lines and the probability curves provide estimates for the probability of fork traversal in HU, assuming *ORI* firing. B) Graphs display P(N)t values for the 300 min simulated HU treatment (see Supplemental Results). This statistic is the fraction of the cell population containing the indicated number of duplicated *CEN*s at each time. Due to the strong down-regulation of *CEN*-proximal *ORI*s, the *dbf4-Δ/pdbf4-zn*simulation displays an initial delay in *CEN* duplication until forks from more distal *ORI*s can converge on *CEN*s. In these graphs, red columns represent the period of spindle assembly as defined in (A).

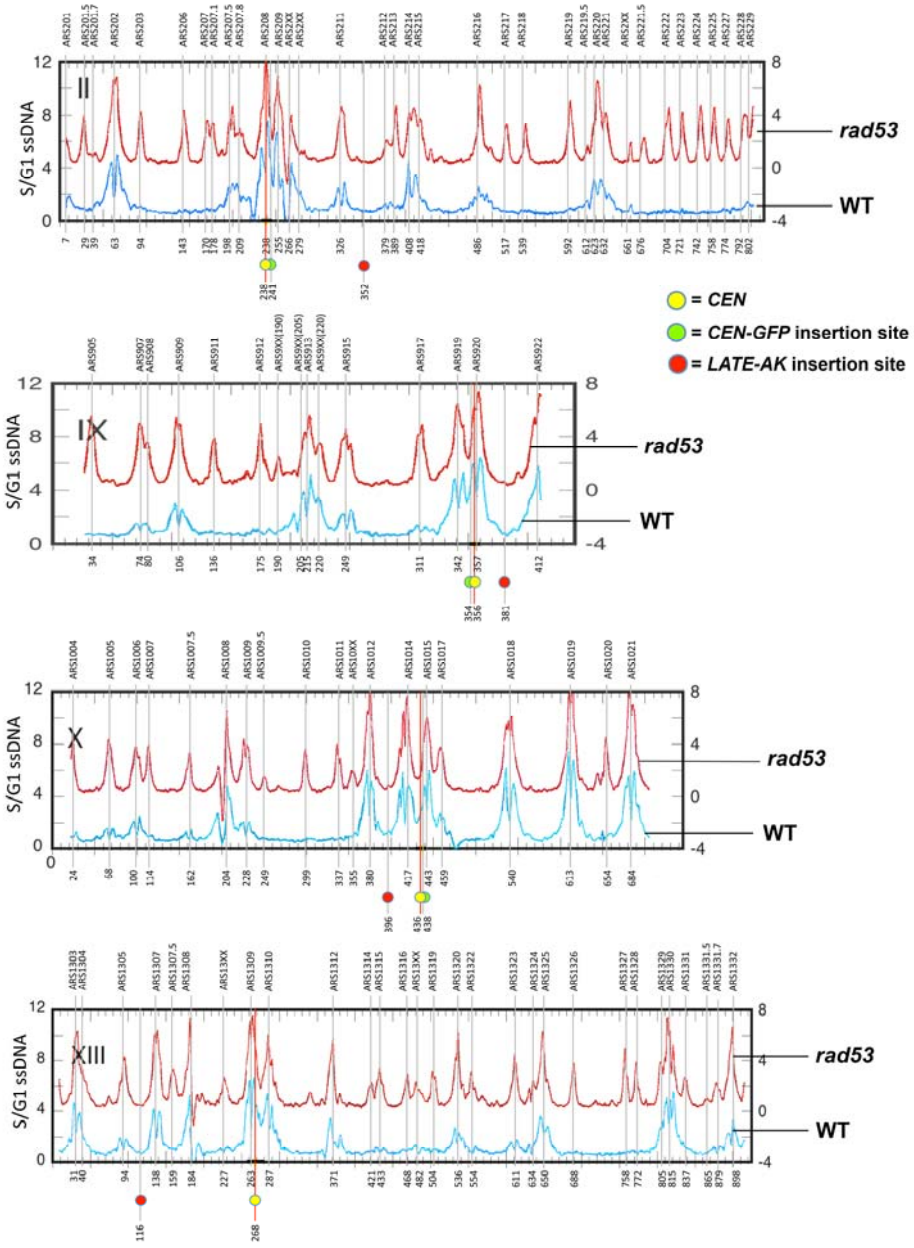

SUPPLEMENTAL FIGURE 6

Supplemental Figure 6.*CEN-GFP*, *LATE-GFP* and *LATE-AK* integrations. Sites selected for *CEN-GFP*, *LATE-GFP* and *LATE-AK*s LacO insertions on chromosomes 2, 9, 10 and 13 are superimposed on the *dbf4-Δ/pDBF4*(WT) and *rad53-21 dbf4-Δ/pDBF4*(*rad53*) replication profiles in HU. *ORI* assignments along the chromosomal axis are also shown. Note that, *CEN-GFP*LacO insertion sites tend to lie near the apex or on the shoulder of *ORI* peaks for *CEN*-flanking *ORI*s. In contrast, sites chosen for *LATE-GFP* and *LATE-AK*LacO insertions are predicted to be maximally distant from unchecked *ORI*s that fire in both WT cells and *rad53* mutants treated with HU. These sites lie in valleys between *ORI* peaks on the replication profiles.

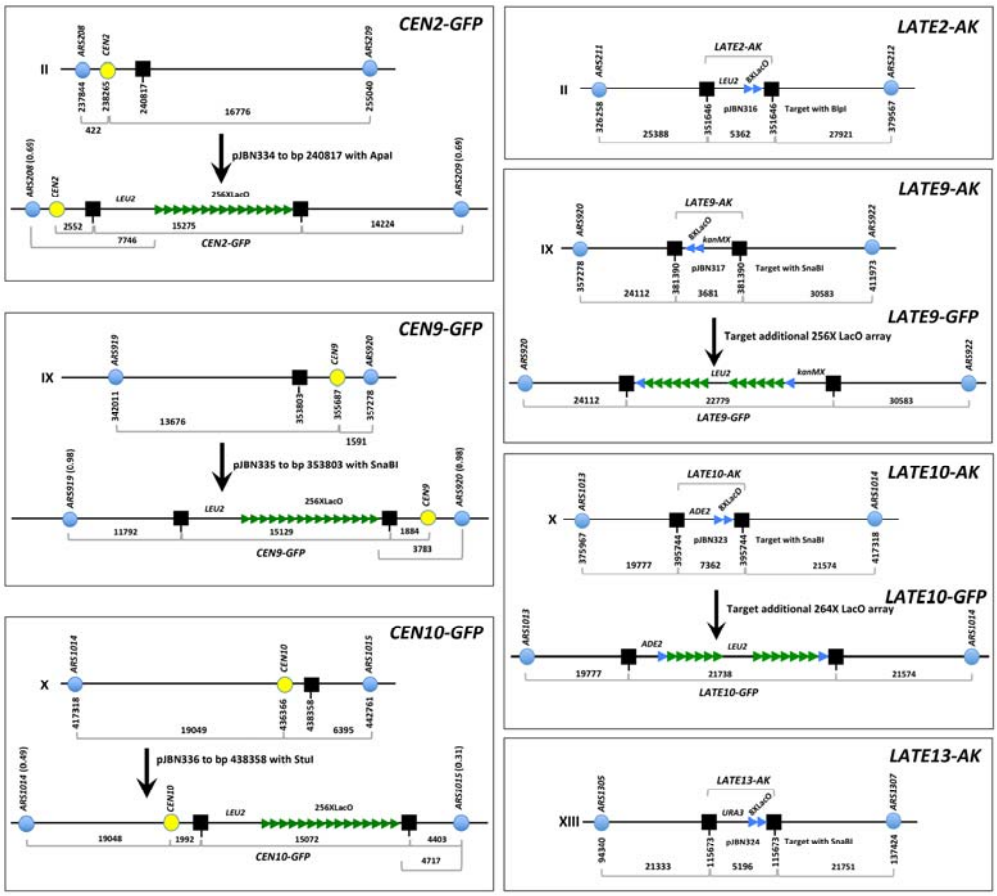

SUPPLEMENTAL FIGURE 7

Supplemental Figure 7.*CEN-GFP*, *LATE-GFP* and *LATE-AK* targetingconstructs. In each panel, yellow circles indicate *CEN*s, blue circles indicate *ORIs* that flank integration sites, and black squares indicate genomic inserts used to target integration. Chromosomal coordinates for *CEN* midpoints, *ORI* midpoints and integration sites are provided. *CEN2-GFP*, *CEN9-GFP* and *CEN10-GFP* diagrams. The upper portion of each panel shows distances (in base pairs) between flanking *ORI*s and the *CEN* prior to integration of the LacO tagging constructs. The bottom portion of each panel illustrates relevant features following integration, including the orientation of the LacO arrays (256 LacO copies, green arrow heads), distances between *CEN*s and insertion sites, distances between the closest flanking *ORI* and the start of LacO array, and relative utilization scores for *CEN*-flanking *ORI*s (Supplemental Table 1). *LATE2-AK*, *LATE9-AK*, *LATE9-GFP*, *LATE10-AK*, *LATE10-GFP*, *LATE13-AK* diagrams.*LATE-AK* constructs introduce 8 copies of LacO (blue arrow heads) to template AK assembly. Distances from the insertion site to the closest flanking *ORI*s are shown. For *LATE9-GFP* and *LATE10-GFP* tagging, homology between AK LacO insertions and 256X LacO tagging constructs was used to target additional LacO arrays for robust GFP tagging, resulting in the configuration of elements shown in each panel.

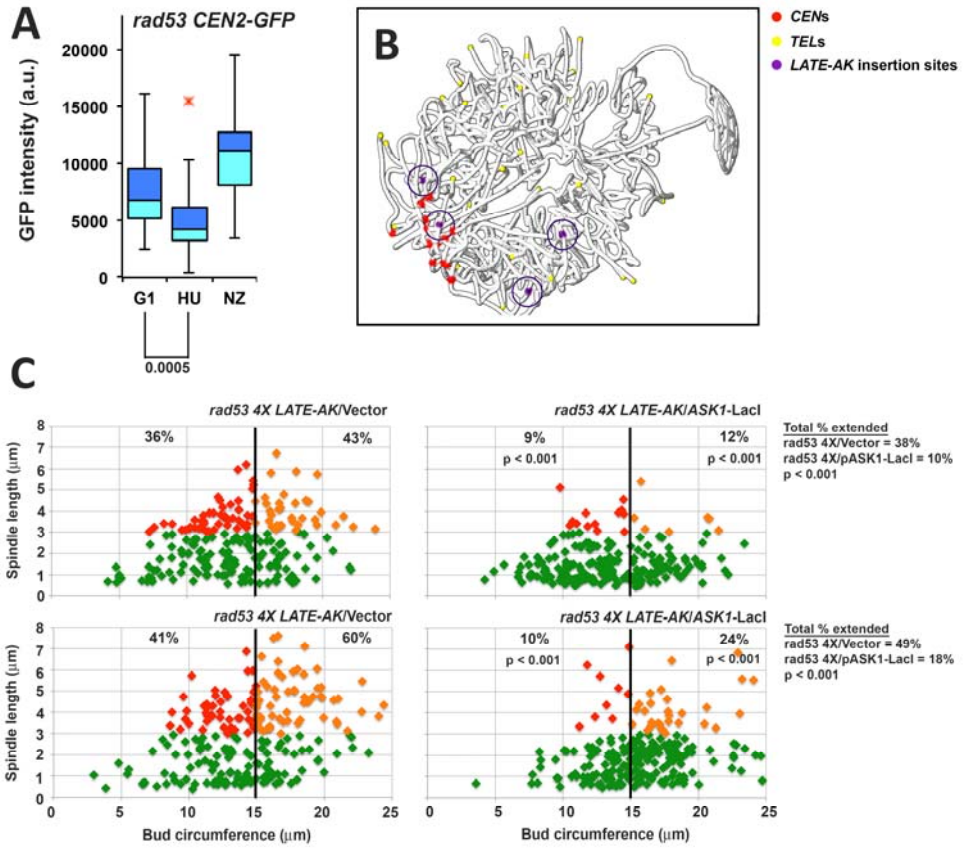

SUPPLEMENTAL FIGURE 8

Supplemental Figure 8. Rad53 regulation of *CEN* DNA integrity and spindle extension in HU. A) *rad53-21 CEN2-GFP* cells (JBY2296) were released from G_1 into media supplemented with 200 mM HU or 15 μg/ml nocodazole (NZ). After 90 min, cells were fixed and scored to quantify *CEN2-GFP* intensity as described in Figure 8. Box plots show distributions for GFP intensity in G_1, HU and NZ treated samples. Results of a two-tailed t-test comparing the signal intensity of the HU sample to the G_1 sample is also provided. B) Spatial map of chromosome organization in the interphase nucleus, showing sites of the four *LATE-AK* insertions (circled in purple). Positions for *CEN*s (red) and *TEL*s (yellow) are also shown. C) Graphs show additional replicates of the experiments described in Figure 9. *rad53-21 SPC42-GFP* strains harboring all four *LATE-AK* insertions (*rad53-214X LATE-AK*; JBY2274 and JBY2275) were transformed with a vector control (pRS413) or a construct expressing *ASK1*-LacI (pJBN321) that activates AK function. Transformants were arrested in G_1 and released into 200 mM HU media at 30°C. After 90 min cells were analyzed for bud circumference and spindle length. Green data points show cells with spindles < 3 μm, red data points show small to medium budded cells (bud circumference < 15 μm) with extended spindles (≥ 3 μm), orange data points show medium to large budded cells (bud circumference ≥ 15 μm) with extended spindles (≥ 3 μm). The percentage of small to medium budded cells with extended spindles and medium to large budded cells with extended spindles is indicated on the charts. p values compare differences in spindle extension between p*ASK1*-LacI transformants with the corresponding region in cells transformed with the vector control. The total percentage of cells with extended spindles, and associated p values, is shown to the right of the graphs. An ~ 4-fold reduction in the frequency of spindle extension is observed in small/medium budded *rad53 4X LATE-AK* cells following activation of the four ectopic MT attachment sites. For medium/large budded cells in the two replicates, the reduction in spindle extension is 3.6- and 2.5-fold, respectively. For total cells, the overall reductions are 3.8- and 2.7-fold. All differences between vector controls and p*ASK1*-LacI transformants are statistically significant.

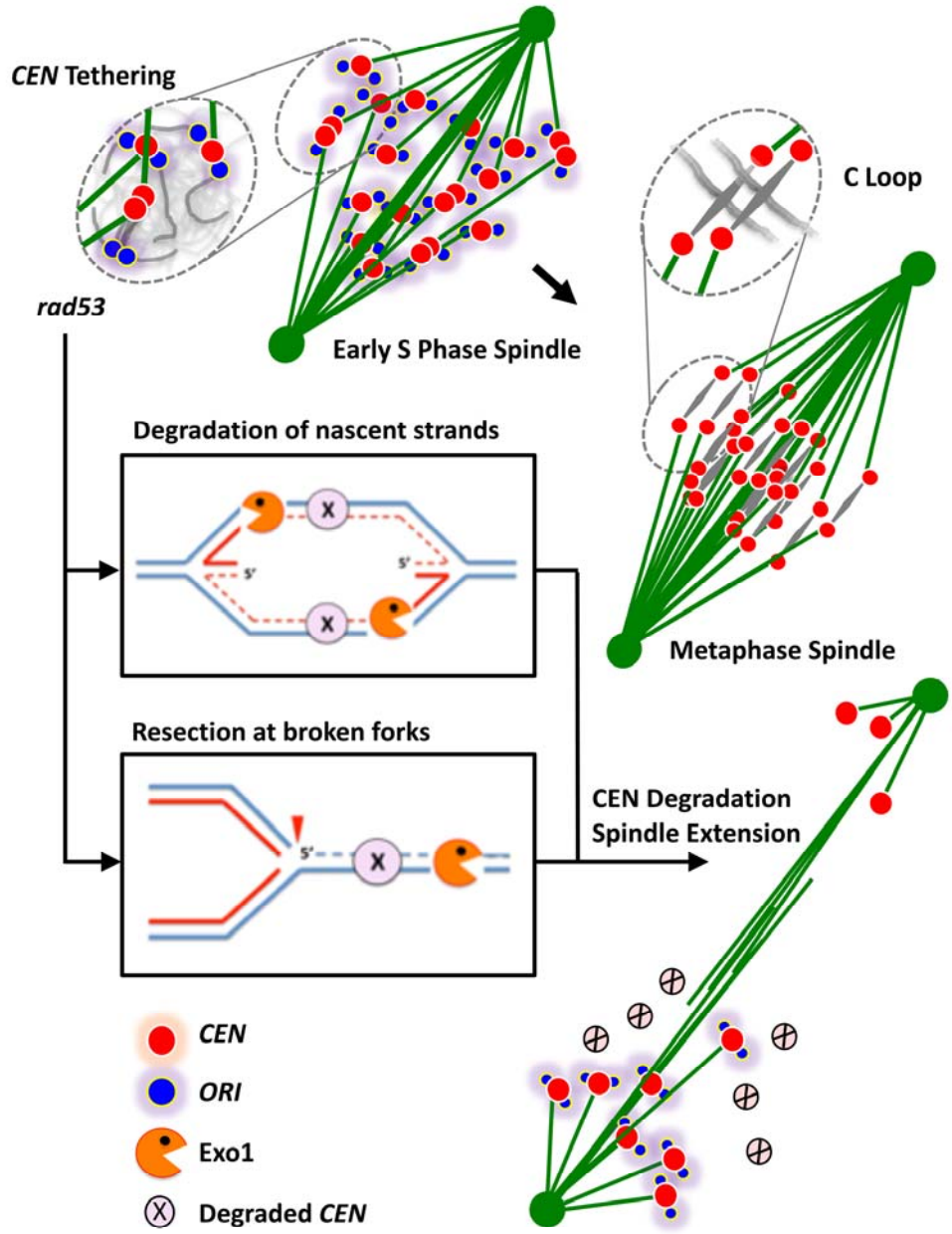

SUPPLEMENTAL FIGURE 9

Supplemental Figure 9.S phase spindle structure and *rad53* spindle extension. A model for a bipolar S phase spindle structure (see also Figure 10B) is shown at upper left. Enlargement illustrates monopolar K-spindle attachments that form prior to *CEN* duplication and precocious amphitelic K-spindle attachments after *CEN*duplication. We envision both types of attachments could generate inward-directed force, possiblydue to their association with replication structures that immobilize S phase chromatin(see text). Given that S phase is thought to be complete before duplicated SPBs separate-at least in rich media-such a bipolar spindle structure may not form unless the relative timing of S phase is extended. This S phase spindle structure would then transition into a typical metaphase spindle configuration as DNA replication proceeds and duplicated sister *CEN*s acquire the capacity to form the C-loop. At this point, each chromatid pair becomes an individualizedtensile element within the spindle (enlarged inset). Such a transition could explain how restraint of spindle extension becomes progressively reliant on Pds1 during the course of a prolonged S phase. As shown in the diagram, in *rad53* mutants treated with HU the formation of aberrant replication fork structures, such as reversed forks, allows Exo1 to degrade nascent strands, leading to loss of *CEN* function (X^{ed}*CEN*s) on one or both presumptive sister chromatids. Alternatively, fork collapse, cleavage of fork ssDNA junctions, or helicase detachment from stalled replisomes, could expose single-stranded nicks, leading to *CEN* degradation ahead of the fork. Loss of a threshold number of K attachments would dissipate inward-directed force, leading to spindle extension. As evaluated by DAPI staining of HU treated *rad53* mutants, a variable-often small-amountof chromatin partitions with the leading spindle pole during extension. Thus, as suggested in the diagram, some *CEN*s may remain competent for spindle attachment but release from replication-associated structures. Alternatively, the immobilized chromatin structure itself may be compromised by loss of the checkpoint.